The effects of consolidation time on the strength and failure behavior of freshwater ice rubble

Hamid Shayanfar [a, b, *], Eleanor Bailey [a], Robert Pritchett [a], Rocky Taylor [a, b]

[a] C-CORE, St. John's, Canada
[b] Memorial University of Newfoundland, St. John's, Canada

ABSTRACT

Medium-scale tests were conducted to measure and observe the strength and failure behavior of freshwater ice rubble. A custom box measuring 3.05 m × 0.94 m × 0.94 m, with Plexiglas walls was built so that failure mechanisms could be observed. Ice rubble beams of nominal thickness 50 cm were produced by placing randomly sized ice pieces into the box filled with water at its freezing temperature. After the specified consolidation time, ranging between 0.2 and 70.5 h, the ice rubble beam was deformed by pushing a platen vertically downwards though the center of the beam until failure. For consolidation times less than 4 h, the ice beam failed progressively and tended to fail by shearing on macroscopic scale. At times greater than 4 h the beam failed by bending. The change in failure behaviour has been attributed to the degree of bonding between ice blocks.

1. Introduction

Ice ridges are large accumulations of ice rubble that form due to compression or shear in the ice cover. They consist of two parts, a sail and a keel. The keel is the submerged part of an ice ridge, which is often frozen at the top forming what is referred to as the consolidated or re-frozen layer. The non-submerged part of the ridge, the sail, is on average one fifth of the keel's depth (Timco et al., 2000). Ice ridges are complex features since they consist of individual ice blocks, random in size and orientation, and are bonded to each other with different degrees of strength from the consolidated layer to the base of the keel. Ridges are the thickest sea ice features in Arctic and sub-Arctic regions, and as such, must be considered during design loads estimation for vessels, offshore structures and subsea infrastructure.

A number of methods have been used to measure the mechanical properties of ice rubble. Initial tests began with the direct shear box test (Keinonen and Nyman, 1978; Prodanovic, 1979; Weiss et al., 1981; Hellmann, 1984; Fransson and Sandkvist, 1985). Timco and Cornett (1999) reviewed these data and suggested that the wide range of data corresponded to the

characteristics of the shear box setup, which induces non-uniform deformation and stress distribution in the ice rubble and forces the sample to fail along an induced failure plane (which may not be the weakest one). Other methods to investigate the mechanics of ice rubble included the shear box tests by Urroz and Ettema (1987), triaxial shear test by Gale et al. (1987) and Wong et al. (1990), biaxial shear tests by Timco et al. (1992), Sayed et al. (1992), Løset and Sayed (1993), Cornett and Timco (1995), and in situ punch tests conducted by Leppäranta and Hakala (1992), Croasdale and Associates Ltd. (1997, 1998) and Heinonen and Määttänen (2000).

Azarnejad and Brown (2001) and Lemee and Brown (2002) conducted laboratory scale punch tests on freshwater rubble to investigate the failure processes under more controlled conditions than are possible in the field. Azarnejad and Brown (2001) examined the influence that beam thickness (0.2 m-0.5 m), consolidation time (0—3 h) and hydraulic ram speed (9—120 mm/s) have on shear strength. They found that with higher consolidation time the cohesion and friction increased due to the development of freeze bonds between ice blocks. They observed that the loading rate influenced both the failure mode and the peak load. At slow loading rates (<40 mm/s), a rectangular or trapezoidal plug of undisturbed ice rubble that spanned the entire thickness was pushed down by the platen and failure occurred mainly at the edges of the plug, while the surrounding rubble remained undisturbed. In comparison, at high deformation rates (45—120 mm/s) the failure occurred over a larger area both under the platen and in the surrounding ice

Nomenclature

η	Porosity
τ	Shear strength
σ	Flexural strength
F_{peak}	Peak load at failure
F_B	Buoyancy force
F_{max}	Maximum net force
ρ_w	Density of water
g	Gravity
δ	Water level displacement
V_b	Nominal volume of submerged ice beam during deformation
V_s	Submerged volume of ice rubble beam before the test (after consolidation)
A	Projected failure area
S	The area of beam deformation at underside of the beam
w	Box width
L	Box length
h	Beam thickness
c	The distance from the edge of the platen to the support/friction bracket
m_{ice}	Mass of ice

rubble. In most cases a triangular or wedge shape was formed and did not span the entire thickness of the rubble beam. Lemee and Brown (2002) carried out similar tests using the same equipment but for larger ice rubble blocks and yielded comparable results. They suggested that ice rubble of larger dimensions failed at higher displacement. They also observed that the lower the initial temperature of the ice blocks, the more bonded the rubble.

In this paper, a series of medium-scale punch tests conducted in C-CORE's cold rooms are described. The focus of this work was to investigate the influence consolidation time had on the strength and failure behaviour of a 50 cm thick rubble beam. Tests consisted of deforming an ice rubble beam by pushing a platen vertically though its center until failure occurs (see Fig. 1). In each case two tests were conducted; the first on the undeformed rubble beam and, the second, on the deformed beam to investigate frictional properties between the ice rubble blocks. The load applied to the platen was measured using a load cell and hydraulic ram displacement with a string potentiometer. Video cameras were strategically positioned around the punch box to observe failure

processes and air and water temperatures measured with Resistance Temperature Detectors (RTDs).

2. Apparatus and instrumentation

A custom-made box has been constructed for the test program that is 3.05 m in length and 0.94 m in width and height. The walls are made from Plexiglas (with a grid drawn on) so that failure mechanisms and ice block motions can be observed and tracked. The platen is rectangular and spans the entire width of the box so that failure mechanisms can be observed. A platen width of 0.4 m was chosen based on careful consideration of how it will influence the failure of the beam and the block dimensions. Load was applied to the platen using a 20,000 lb (9 ton) hydraulic ram. To help make beams of even geometry, a bottom plate, mounted on 4 threaded rods, was brought up to produced beams that were 50 cm in thickness (see Fig. 2).

During tests where the rubble was heavily bonded, the buoyancy of the non-loaded portion of the rubble was not sufficient to resist the applied load. As such, brackets had to be added to the end of the box to cause the beam to fail. This is similar to the procedure used by Azarnejad and Brown (2001) and Lemee and Brown (2002) where they glued small Plexiglas pieces on the tank walls to artificially increase friction between the tank walls and the ice rubble. The only difference being here that friction was only added to the ends of the box rather than the whole box to allow beams to fail in bending as well as shear.

A load cell was placed in line with the hydraulic ram to measure force applied to the rubble. A string pot was used to measure the vertical displacement and velocity throughout indentation. A total of six cameras were used to observe the tests from different views. Four were placed side-on to view the test through the Plexiglas window and two from the top (see Fig. 3). A high speed video camera (HSV) was used to view the mid-point of the beam where the failure planes occurred, which is needed for calculating the shear strength. Three LED work lights were mounted on the opposite side of the box to illuminate the ice rubble beam. Cameras were syncronized with the load and displacement data through a noise trigger.

Five (5) RTDs were used to measure air and water temperatures. Three (3) RTDs were placed in the water, two directly underneath the ice rubble beam (one at the centre of the box and the other at one end) and one at the bottom of the box (see Fig. 1). Two (2) RTDs were also placed in the air to measure cold room temperature at different locations. The RTDs' measurements were logged at a sample rate of 1 min, starting from the time that the box was filled
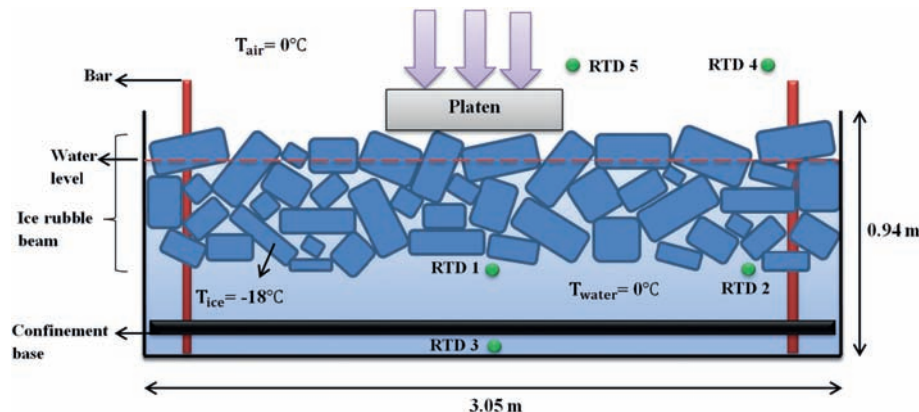

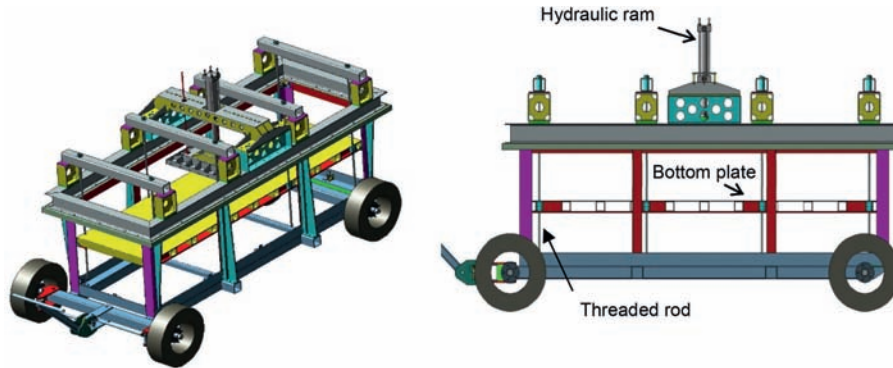**Fig. 1.** Schematic showing the test setup.

Fig. 2. Computer aided design (CAD) images of the testing assembly.
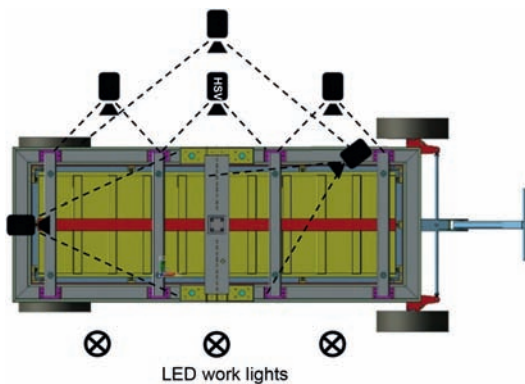

Fig. 3. Camera and lighting locations.

with ice rubble.

3. Ice rubble production

Freshwater ice rubble was produced and stored in a refrigerated container. 1 m² pans were filled with tap water to an approximate depth of 10 cm and left to freeze at a nominal temperature of −18 °C. Two dividers were placed in each pan prior to freezing to facilitate ice breakage. Once the water was frozen (approximately 5–6 days), pans were manually flipped over, allowing ice to break into randomly sized ice pieces. Larger sized ice pieces were broken with a hammer to give target lengths between 10 cm and 50 cm. Very small fragments and powdered ice which were less than 10 cm in thickness were swept away and thrown out. Fig. 4 shows photographs of the reefer unit and the ice production methodology.

An analysis of the ice block dimensions was carried out to determine the ice block length, width and volume distributions.

Photos of the ice blocks were taken during ice rubble fabrication and later analyzed using image processing software. Fig. 5 shows that the length distribution of the ice blocks varied between 10 and 70 cm, with the majority falling in the range of 30–40 cm. The width distribution varied from 10 to 50 cm, with almost 60% of the blocks being between the ranges of 20–30 cm. The length to width ratio distribution shows that the ice blocks are generally square in shape with a maximum length to width ratio between 1 and 1.5.

In Table 1 a summary of the ice blocks dimensions measured in first-year sea ice ridges (after Strub-Klein and Sudom, 2012) and previous laboratory tests are given. Only selected laboratory tests are given here, the reader is referred to tables presented by Bruneau (1997), Brown and El Seify (2005) and Liferov and Bonnemaire (2005) for additional data. The mean length, width and thickness of the ice blocks measured in the field are much larger than those used in previous laboratory tests. Ice rubble for laboratory tests are typically scaled by a factor on the order of 10–30 times as compared to full-scale block sizes. By scaling the rubble the thermodynamic properties are altered, which will undoubtedly alter the strength and failure behaviour of the rubble. Liferov and Bonnemaire (2005) compared laboratory and field punch tests load curves and suggested that the lack of a distinct peak observed in those laboratory tests may have been caused by inappropriate thermodynamic scaling of rubble. The consequence of which resulted in a less bonded rubble matrix. As a result in these tests relatively "large" ice blocks were used (at least in the context of laboratory tests), as we believe this to be an important parameters when investigating the influence of consolidation time on the strength and failure behaviour of ice rubble.

4. Testing procedure

Approximately 750 kg of ice rubble were needed to produce a 50 cm thick ice rubble beam. Bags were transported via forklift

Fig. 4. Ice rubble production and storage inside the refrigerated container.
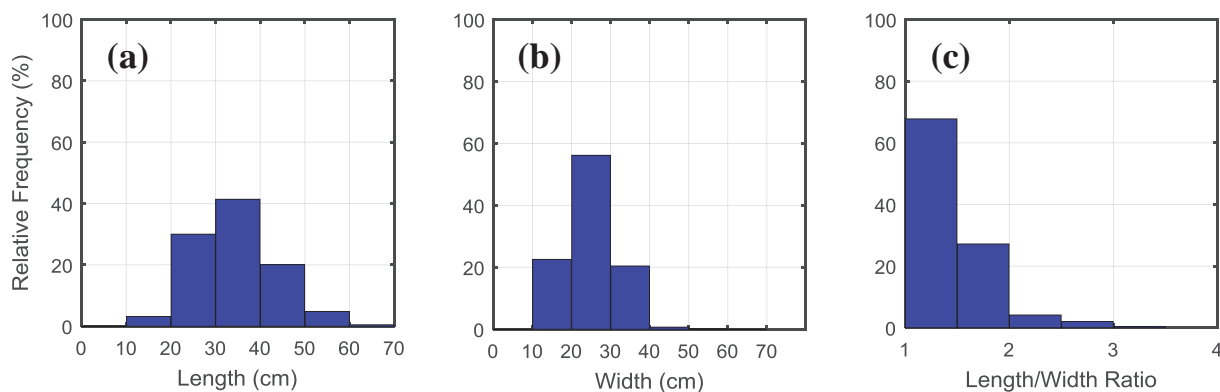
Fig. 5. Histograms of the length (a), width (b) and length to width ratio (c) of the ice blocks.

Table 1
Summary of ice block dimensions as for field tests (after Strub-Klein and Sudom, 2012) and selected laboratory tests.

Field tests			
Location	Thickness (m)	Width (m)	Length (m)
Baltic Sea	0.24	0.71	0.92
Barents Sea	0.67	0.88	9.47
Beaufort Sea	0.71	1.12	1.21
East Coast of Canada	0.26	1.08	1.35
Svalbard [a]	0.35	0.68	0.96
Laboratory tests[b]			
Azarnejad and Brown (2001)	0.075	0.15	0.2
Lemee and Brown (2002)	0.025	0.1	0.15
Serré et al. (2011)	0.022	0.04	0.06

[a] Shafrova and Høyland (2008).
[b] Only the maximum sample dimensions of this study is shown here.

Table 2
Test matrix.

Test No.	Consolidation time (hours)	Initial ice temperature (°C)	Block size
1	0.2	−18	(Length 30—40 cm; Width 20 —30 cm)
2	2.4		
3	4.2		
4	4.4		
5	10.1		
6	28.5		
7	70.5		

from the refrigerator container to C-CORE's Centrifuge bay area (just outside the cold room), where they were loaded into the box with the use of an overhead crane. The mass of each ice rubble bag was measured using the crane scale, which is needed to derive porosity. Whilst loading the ice rubble into the punch box the bottom plate was positioned 50 cm from the top of the box, which helped to produce a beam of even geometry. Care was taken during beam construction to ensure that the ice blocks were evenly positioned under platen so that no block was protruding beyond the beam surface which might cause premature failure of the beam.

Once the ice rubble beam was prepared, the bottom plate was lowered allowing the rubble beam to float in hydro-static equilibrium. The box was then moved back into the cold room where the ice rubble blocks were left to consolidate for a set period of time. On average the cold room temperature fluctuated between 2 °C and −0.6 °C during the consolidation period (see Fig. 6 which shows the water and air temperature measured by the RTDs during Test 6). With the exception of the first 150 min, the water temperature

remained constant during the entire consolidation period. The temperature measured by RTD 3 (located towards the bottom of the punch box − see Fig. 1) was 0.8 °C warmer than that reported by RTD 1 (located just under the rubble beam), indicating that the water was stratified. RTD 2 was marginally colder (0.26 °C) than RTD 1, as it was located towards the edge of the box. In the first 150 min, there were some fluctuations in the water temperature caused by mixing of the stratified water column, as the bottom confinement plate was lifted and dropped when fabricating the ice rubble beam.

Two tests were carried out on each ice rubble beam: 1) punch test and 2) friction test. The punch test on the ice rubble beam was completed by deforming it at a constant rate of 5 mm/s until the beam failed. After each punch test, the hydraulic ram was retracted, allowing the failed rubble beam to settle back to hydro-static equilibrium. A second test was then performed on the same beam, that was referred to as the friction test, as it was assumed that all bonds would have failed in the previous punch test and as such would be a measure of the friction and interlocking between ice rubble blocks. It is worth noting that the friction test was rapidly conducted after the punch test so that no new freeze bonds would have formed. The main purpose of the friction test was for comparison with the punch test so that the influence of the freeze bonds on the strength of the beam could be compared with the frictional (and buoyant) component.

A total of seven punch tests were carried out to investigate the influence consolidation time had on the strength and failure behaviour of an ice rubble beam (see Table 1). The consolidation time was varied from 0 to 70.5 h, whilst the initial ice temperature was held constant at −18 °C. Note that while best efforts were made to conduct the test in "0 h" the fastest test setup time that has actually been achieved was 0.2 h (12 min).

5. Results

Analysis of the video and load data from the test carried out after 0.2 h of consolidation (see Fig. 7) showed that a shear plug failure took place. Failure of the shear plug was progressive, where the first failure (marked 1 in the figure) took place to the right of the platen at 53 mm of displacement, followed by a second failure (marked 2 in the figure) to the left of the platen at 85 mm of displacement. The load trace from the friction test showed that no load drops were observed, demonstrating that as expected, the loads were associated with frictional and buoyancy forces with little or no bond failure. The higher loads observed in the punch test are likely due to a combination of interlocking between ice blocks or potentially some initial freeze bondings that may have taken
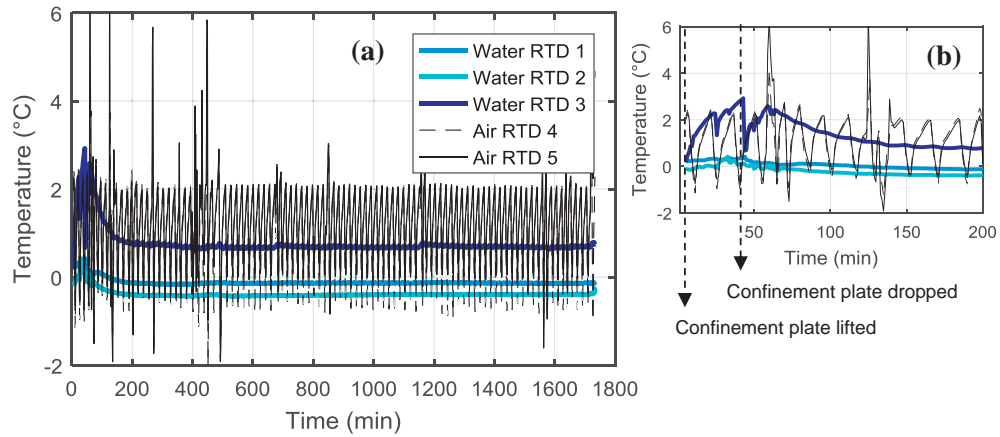
Fig. 6. Water and air temperatures measured by the RTDs for Test 6 showing (a) entire test; (b) first 200 min.
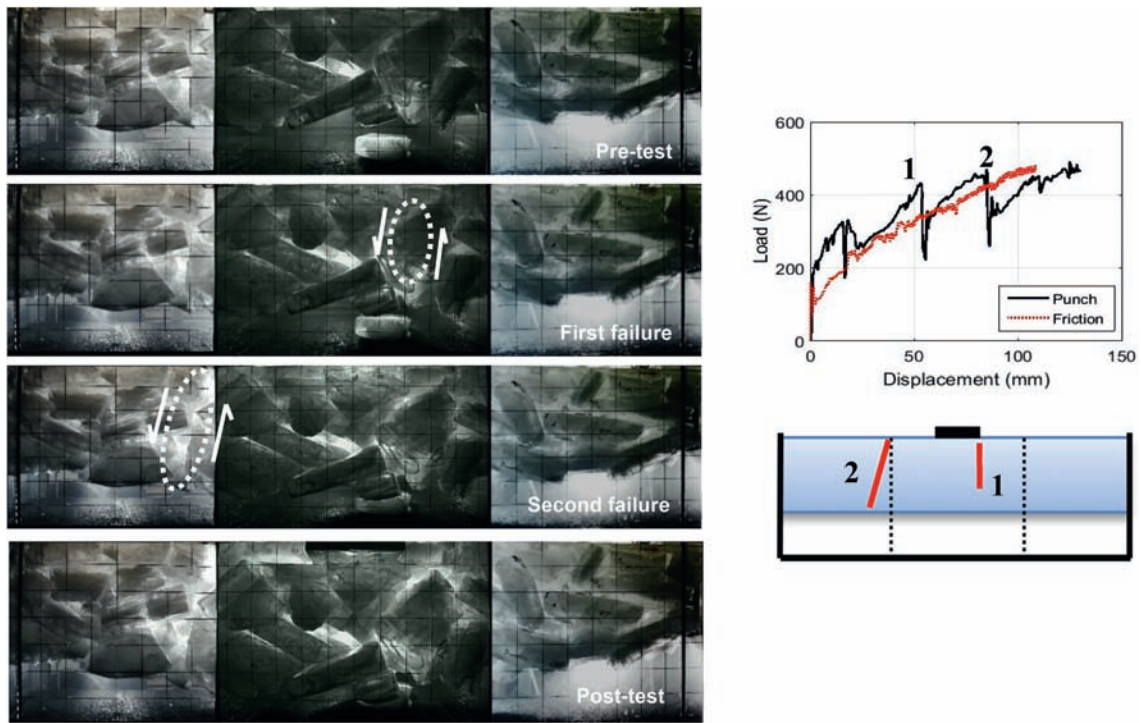

Fig. 7. Analysis of video and load data from Test 1, which had a consolidation time of 0.2 h, an initial ice temperature of −18 °C, and an ice rubble beam thickness of 50 cm (see Table 2).

place in the time it took to setup and run the test. The increase in load observed with displacement in both the punch and friction tests is due to increasing buoyancy forces as the ice beam is submerged further below the water.

The failure behaviour observed in the test conducted after 70.5 h of consolidation (see Fig. 8), was noticeably different from that done at 0.2 h, where the beam failed in bending as opposed to shear. The load trace measured during the punch test showed a single failure (marked 1 in the figure) at 65 mm of displacement. The failure plane was located slightly to the left of the platen, as opposed to the center which would be the case if the beam was homogenous. This is not unexpected as the distribution of the ice blocks in the rubble beam is random resulting in a non-uniform stress distribution. The loads measured in 70.5 h friction test were significantly lower than those measured in the punch test,

especially during peak load. This is because the rubble beam was heavily bonded in the punch test which increased the strength of the beam, whereas in the friction test, the bonds along the failure plane had already been broken.

Fig. 9 compares the ice rubble beam deformation at the end of Tests 1 and 7, in which the dashed and dotted lines show the position of the beam before and after the test, respectively. Note that the top of the beam was just above the viewing panel at the start of the test, therefore no dashed line is given at the top of the beam for the pre-test position. Fig. 9(a) demonstrates that at low consolidation times (0.2 h), the ice rubble failure mode is more analogous to shear plug failure where the central part of the beam (the plug) was displaced while the non-loaded portion of the beam remained in place. The amount of displacement at the top and bottom of the beam was approximately constant indicating that there was little
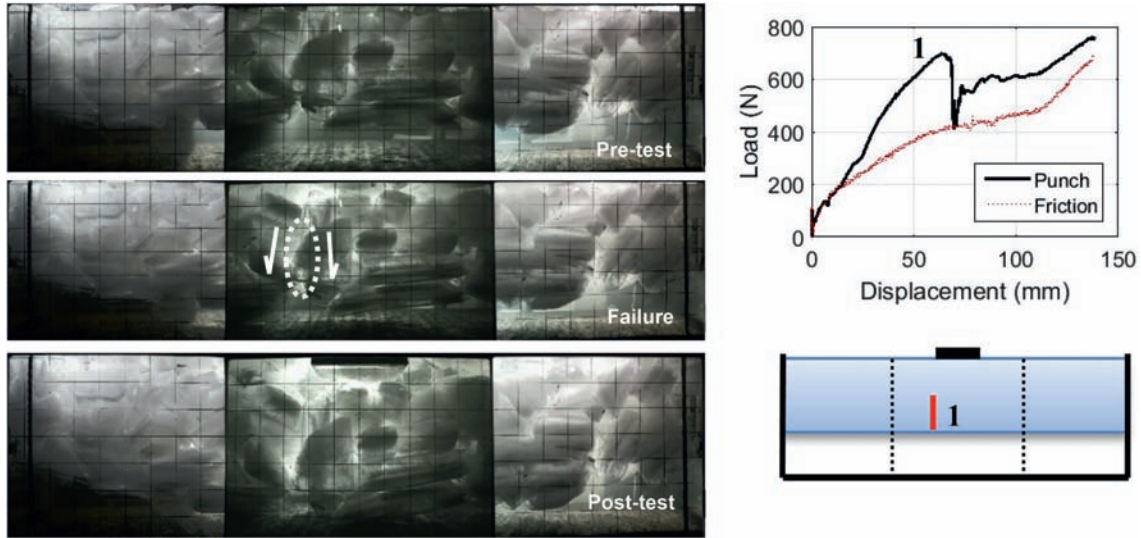
Fig. 8. Analysis of video and load data from Test 7, which had a consolidation time of 70.5 h, an initial ice temperature of −18 °C, and an ice rubble beam thickness of 50 cm (see Table 2).
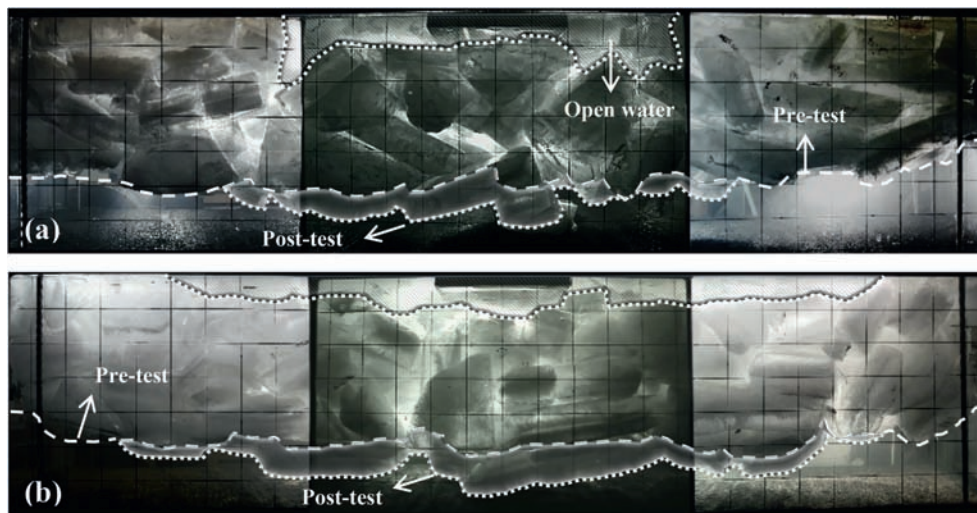

Fig. 9. Comparison of the failure behaviour of the ice rubble beam during the punch tests, (a) after 0.2 h consolidation (Test 1), (b) and 70.5 h consolidation (Test 7).

movement/interlocking of the rubble and failure was predominantly shear along the plug interfaces. A couple of the ice blocks at the top of the beam that weren't in contact with the platen floated up to water surface as the plug was submerged. In contrast, Fig. 9(b) shows that at higher consolidation times (70.5 h), the rubble both under the platen and surrounding rubble beam was displaced. The displacement at the centre of the beam was greater than at edges and localized tensile failure where observed at the base of the beam in some tests. This suggests that the beam was more heavily bonded, allowing a greater amount of stress to be transmitted through the beam causing it to fail at greater displacements in bending/flexural failure.

Fig. 10 shows the load-displacement traces for all punch and friction tests, as well as a schematic showing the observed failure behaviour of the beam. A failure was characterized by a load drop synchronized with an observed displacement in the rubble. For consolidation times less than 4.4 h, the beam failed progressively in shear, where there were two large load drops observed before plug failure. For these shorter submersion times, since the bonds are

expected to be weaker, a progressive sequence of block-block failures characteristic of macroscopic shear failure is more likely, which is analogous to shearing of a cohesive granular material. After 4.4 h of consolidation, the deformation behaviour appeared to change to a combination of bending and shearing or pure bending, where a single load drop resulted in failure of the beam. This behaviour may be attributed to increasing bonding which causes the rubble matrix to take on the behaviour of a brittle porous solid, in which higher stresses can be transmitted throughout the matrix resulting in macroscopic beam-like behaviour characterized by flexural failure. No schematic showing the observed failure area is given for Test 3 as the video malfunctioned. We believe, however, that failure was progressive and took place at points 1 and 2 marked on the load-displacement curve. The peak load at failure increased with consolidation time from 430 N in the 0.2 h test to 1400 N in the 4.4 h test, after which, it reduced to 700 N after 28.5 h of submersion. It is interesting that the 4.2 h test was much lower than the 4.4 h test, which was essentially a repeat test. This is possibly due to differences in setup times, which caused the beam
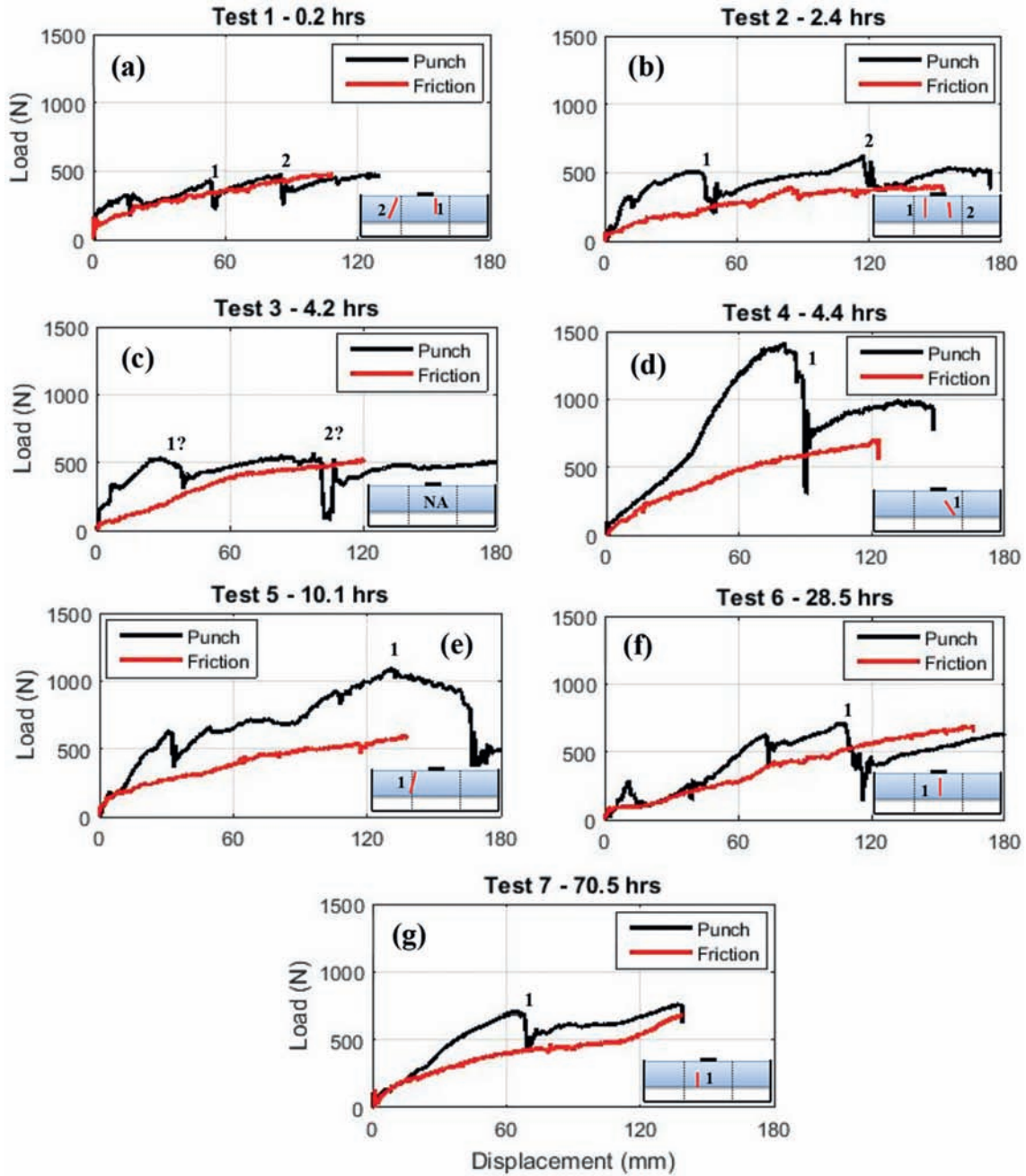
Fig. 10. Load-displacement plots for all the punch and friction tests.

to be less bonded and hence alter the failure mode or differences in the distribution of the blocks between the two tests which may have resulted in interlocking. Additional repeat tests are needed to understand this discrepancy in more detail.

In Fig. 11 the load traces for each fiction test are plotted on the same figure to determine if a relationship is evident for the different consolidation times. In general, an almost linear relationship exists between the frictional force and platen displacement. Buoyancy is believed to contribute to the linear increase in the friction forces, whereby with greater beam displacement a greater percentage of the beam will be submerged. In addition, the failure mode appears to influence the frictional force where at consolidation times greater than 4.2 h (Tests 4 to 7), when beam bending failure was observed, greater loads were measured at the

end of the test. Conversely, in tests where the consolidation time was less than 4.4 h (Tests 1 to 3) and shear failure was prominent lower loads were recorded at the end of the test. This is because when failing in bending a greater portion of the beam is submerged than when failing in shear. In Test 2, it was observed that after 80 mm of displacement the frictional force gradually levelled off to a constant value. This because past 80 mm of displacement the plug was completely submerged below the water causing buoyancy to become constant.

6. Data analysis

In order to measure the shear and flexural strength of ice rubble beam, the buoyancy force must be calculated for each test. Two
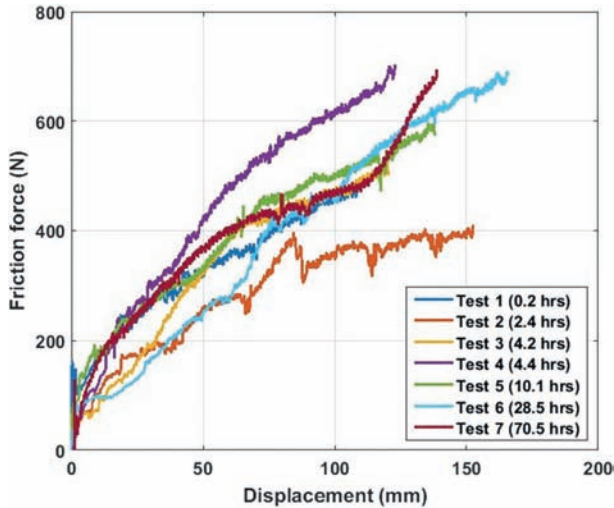
Fig. 11. Load-displacement plots for the friction tests.

methods have been used to calculate the buoyancy force at the time of beam failure. In the first method, the rise in water level, δ, was used to estimate the buoyancy force (F_B) at failure,

$$F_B = \delta w L \rho_w g \quad [N] \tag{1}$$

where ρ_w is the density of water, g is gravity and w and L are width and length of the box, respectively. δ was estimated from the height of the water level before the test (y_0) and at beam failure (y) i.e. $\delta = y - y_0$ (see Fig. 12a). In the second method, the displacement observed at the underside side of the beam was used to estimate the buoyancy force at failure,

$$F_B = (1 - \eta) \rho_w g V_b [N] \tag{2}$$

where V_b is the nominal volume of the displaced ice beam and η is the macro porosity of the rubble beam. V_b was determined from the video data where the position of the underside of the beam pre- and post-failure are shown in solid and dotted lines, respectively (see Fig. 12b). It is the product of the length- displacement plot area (S in Fig. 12b) and the box width. Note that this method assumes

that the displaced volume at the underside of the beam is equal to the submerged volume at the top of the beam (i.e. no compaction or expansion took place).

The porosity of the beam was derived from the following,

$$\eta = 1 - \frac{m_{ice}}{\rho_w V_s} \tag{3}$$

where $m_{ice} = 750$ kg was the mass of the ice and V_s was the volume of the submerged portion of the beam. V_s was estimated from the video data by measuring the distance from the water level to the bottom of the beam. Since the videos were only setup immediately prior to deforming the beam, Eq. (3) therefore gives the porosity after consolidation.

The estimated buoyancy force at failure was calculated for each test using both method I and II (Table 3). Results for both methodologies are presented here, not only for comparison, but also because in Test 3 one of the cameras malfunctioned so we were not able to observe the full beam and in Test 6 the water level was above the viewing panel. The buoyancy forces estimated using both methodologies were similar for all tests with the exception of Test 5. We are uncertain why the buoyancy force calculated using method II in Test 5 was higher than that calculated using method I. It was, however, noted that in this test the beam failed at a much greater ram displacement. This could have resulted in greater tensile splitting at the bottom of the beam resulting in an increased porosity (which was assumed to be constant in Eq. (2)). As a result it is believed that method I was more accurate and hence was used as the preferred method in the shear/flexural strength calculations (with the exception of Test 6 where method II was used). Table 3 shows that with increasing hydraulic ram displacement the buoyancy force increases.

The shear strength of the ice rubble beam was estimated from the following equation,

$$\tau_{shear} = \frac{F_{Max}}{A} = \frac{F_{peak} - F_B}{A} \quad [kPa] \tag{4}$$

where A is the failure area and F_{Max} is the maximum net force calculated by taking the peak force at failure minus the buoyancy force. For all tests (with the exception of Test 3) A was estimated from the video data by taking the observed failure plane at peak load and extending it over the full thickness and width of the beam

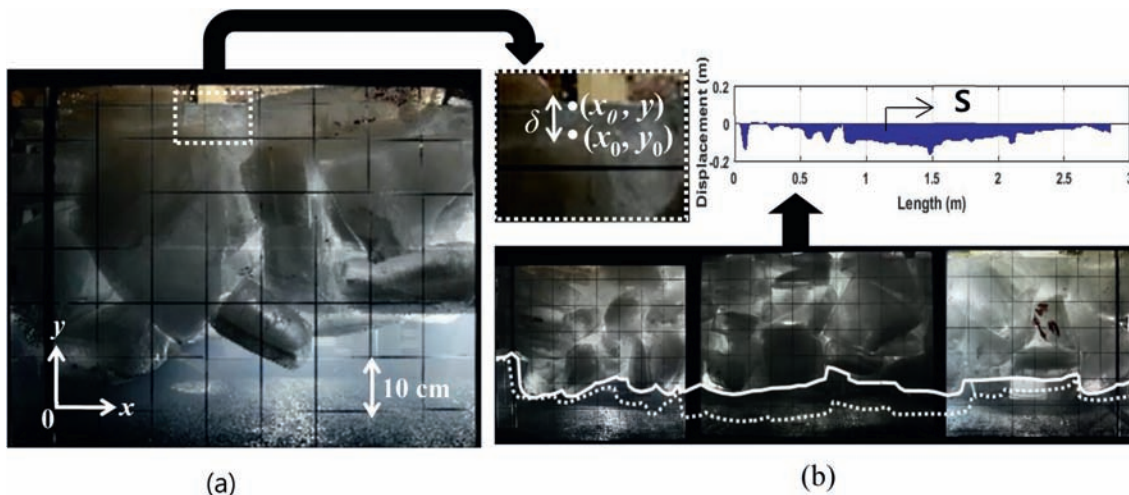**Fig. 12.** Snap shots of the video data showing how the water level displacement (δ) and the displaced beam volume (V_b) were estimated for the buoyancy force calculations used in method I (a) and method II (b), respectively. Note that the grid on the box is 10 cm^2.

(as illustrated in Fig. 10). As no video data was recorded in Test 3 a nominal area of 0.47 m² was used based on the width and thickness of the beam.

The flexural strength of the beam was estimated using the four-point beam bending equation, as it was observed that at higher beam deflection the load was transmitted to the edges of the platen rather than point loaded in the centre. The flexural strength was derived after Schwarz et al. (1981),

$$\sigma_{flexural} = \frac{3F_{max}c}{wh^2} \, [\text{kPa}] \qquad (5)$$

in which, w and h are the width and thickness of the ice beam, respectively, and $c = 1.325$ m is the distance from the edge of the platen to the support/friction bracket.

In Table 4, the shear and bending strengths for different consolidation times are given, as well as the observed failure mode, maximum net force and estimated failure area. In Fig. 13 the calculated shear and flexural strength values are plotted as a function of consolidation time. Both plots show similar trends

where the strength remained roughly constant from 0.2 h to 4.2 h, after which there was a jump in load which gradually decreased until 70 h. The only noticeable difference between the two curves is after 4.2 h, where the magnitude of the increase at 4.4 h was less for the shear strength calculations. This was because the observed failure area was used in the shear strength calculations, as opposed to the flexural strength calculations assumed a constant area.

7. Discussion and conclusion

A total of seven tests were conducted to investigate the influence that consolidation time has on the strength and failure behaviour of a 50 cm thick freshwater ice rubble beam. Results showed that as the consolidation time varied from 0.2 h to 70.5 h, the failure behaviour changed considerably. For consolidation times less than 4.4 h, the ice beam failed progressively and tended to fail by shearing on macroscopic scale, whereas at times greater than 4.4 h the beam failed in a combination of shearing and bending or pure bending. The change in failure behaviour is controlled by the

Table 3
Estimated buoyancy force at peak load.

Test No.	Consolidation time (hrs)	Hydraulic ram displacement (mm)	Porosity	Buoyancy force (N)	
				Method I	Method II
1	0.2	52.8	0.39	290	156
2	2.4	41.4	0.37	408	432
3	4.2	29	–	439	–
4	4.4	80.6	0.39	682	611
5	10.1	132.1	0.44	695	920
6	28.5	106.5	0.42	–	449
7	70.5	64.25	0.38	504	514

Table 4
Estimated shear/bending strength at peak load.

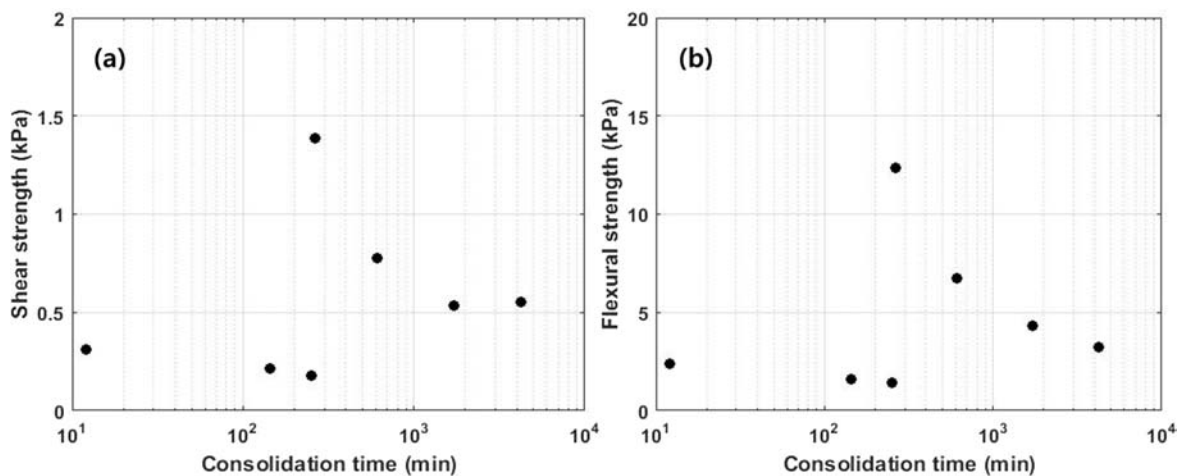| Test No.	Consolidation time (hrs)	Observed mode of failure	F_{Max} (N)	A (m²)	τ_{shear} (kPa)	$\sigma_{flexural}$ (kPa)
1	0.2	Shear	141	0.46	0.31	2.39
2	2.4	Shear	93	0.43	0.21	1.57
3	4.2	Shear (?)	83	0.47	0.18	1.4
4	4.4	Bending	732	0.53	1.39	12.4
5	10.1	Bending	398	0.51	0.78	6.73
6	28.5	Bending	255	0.48	0.54	4.31
7	70.5	Bending	192	0.35	0.55	3.25

Fig. 13. Shear (a) and flexural (b) strength vs. consolidation time.

degree of bonding between ice blocks, where at low consolidation times the rubble was less bonded and behaved more like a cohesive granular material failing as a shear plug (see Fig. 9). At greater consolidation times the increased bonding caused the rubble to behave like a porous solid. At the microscopic scale this implies that when bonded the freeze bonds in the rubble would fail in compression and tension, as well as shear, which was observed in the video (see Fig. 9).

Due to the different failure modes observed, the data were analyzed both in terms of a shear and flexural strength. At low consolidation times (0—4.2 h), the shear strength of the rubble varied from 0.31 kPa to 0.18 kPa with an average of 0.25 kPa. These are similar to the values report by Azarnejad and Brown (2001), which is surprising considering the different test setup, block size dimensions, initial ice temperatures and ram speeds. At higher consolidation times (4.4—70.5 h), the flexural strength varied from 3.25 kPa to 12.4 kPa with an average of 7.8 kPa. Since these were the first tests which measure the flexural strength of an ice rubble beam there is no data with which to compare.

Given the results presented here it is clear that the failure behaviour of the rubble changes considerably with consolidation time. In such cases it may not be correct to assume the rubble fails in pure shear, as is currently done in most ice ridge loading models, but rather a combination of shear and/or bending. Understanding the flexural properties of rubble may be particularly important when considering rubble and ridge interactions with sloping structures or vessels. In the new model proposed by Croasdale (2012) the load from a first-year sea ice ridge on a sloping structure is determined using composite beam theory. For this information about the modulus and flexural strength (tensile or compressive failure) of rubble needed. Further work in the area is ongoing to investigate these processes in more detail.

Acknowledgements

References

Azarnejad, A., Brown, T., 2001. Ice rubble behavior in punch test. J. Cold Reg. Eng. 15 (3), 135—153.

Brown, T., El Seify, M., 2005. A Unified Model for Rubble Ice Load and Behaviour. NRC Publications Archive, Canada.

Bruneau, S., 1997. Development of a First-year Ridge Keel Load Model. PhD thesis. Memorial University of Newfoundland, St. John's, Newfoundland, Canada.

Cornett, A., Timco, G., 1995. Laboratory Tests on the Mechanical Properties of Saline Ice Rubble. NRC Report HYD-CTR-002, p. 171.

Croasdale & Associates, 1997. In Situ Ridge Strength Measurements. A Study Sponsored by NRC (PERD) and Exxon Production Research Co.

Croasdale & Associates, 1998. In Situ Ridge Strength Measurements. A Study Sponsored by NRC (PERD) and Exxon Production Research Co.

Croasdale, K.R., 2012. A simple model for first-year ridge loads on sloping structures. In: Proceedings. IceTech, Banff.

Fransson, L., Sandkvist, J., 1985. Brash ice shear properties - laboratory tests. In: Proceedings of the 8th International Conference on Port and Ocean Engineering under Arctic Conditions, vol. 1, pp. 75—87. Narssarssuaq, Greenland.

Gale, A., Wong, T., Sego, D., Morgenstern, N., 1987. Stress-strain behavior of cohesionless broken ice. In: Proceedings of the 9th International Conference on Port and Ocean Engineering under Arctic Conditions, vol. 3, pp. 109—119. Fairbanks, AK.

Heinonen, J., Määttänen, M., 2000. LOLEIF ridge-loading experiments-analysis of rubble strength in ridge keel punch test. In: Proceedings of the 15th International Symposium on Ice, vol. 1, pp. 63—72. Gdnask, Poland.

Hellmann, J., 1984. Basic investigations of mush ice. In: Proceedings of the 7th International Symposium on Ice, vol. 3, pp. 37—55. Hamburg, Germany.

Keinonen, A., Nyman, T., 1978. An experimental model-scale study on compressible,frictional and cohesive behavior of broken ice masses. In: Proceedings of the International Symposium on Ice, vol. 2, pp. 335—353. Lulea, Sweden.

Lemee, E., Brown, T., 2002. Small-scale plane strain punch tests. In: Proceedings of the 16th IAHR International Symposium on Ice, vol. 2, pp. 1—8. Dunedin, New Zealand.

Leppäranta, M., Hakala, R., 1992. The structure and strength of first-year ridges in the Baltic Sea. Cold Reg. Sci. Technol. 20, 295—311.

Liferov, P., Bonnemaire, B., 2005. Ice rubble behaviour and strength: Part I. Review of testing and interpretation of results. Cold Reg. Sci. Technol. 41, 135—151.

Løset, S., Sayed, M., 1993. Proportional strain tests of fresh water ice rubble. Cold Reg. Sci. Technol. 7 (2), 44—61.

Prodanovic, A., 1979. Model tests of ice rubble strength. In: Proceedings of the 5th International Conference on Port and Ocean Engineering under Arctic Conditions, pp. 89—105. Trondheim, Norway.

Sayed, M., Timco, G., Lun, L., 1992. Testing ice rubble under proportional strains. In: Proceedings of Offshore Mechanics and Arctic Engineering Conference, pp. 335—341. Calgary, Canada.

Schwarz, J., Frederking, R., Gavrillo, V., Petrov, I.G., Hirayama, K.I., Mellor, M., Tryde, P., Vaudrey, K.D., 1981. Standardized testing methods for measuring properties of ice. Cold Reg. Sci. Technol. 4, 245—253.

Serré, N., Repetto-Llamazares, A.H., Høyland, K.V., 2011. Experiments on the relation between freeze-bonds and ice rubble strength, Part I: Shear box experiments. In: Proceedings of the 21st International Conference on Port and Ocean Engineering under Arctic Conditions, Montreal, Canada.

Shafrova, S., Høyland, K.V., 2008. Morphology and 2D spatial strength distribution in two Arctic first-year sea ice ridges. Cold Reg. Sci. Technol. 51, 38—55.

Strub-Klein, L., Sudom, D., 2012. A comprehensive analysis of the morphology of first-year sea ice ridges. Cold Reg. Sci. Technol. 82, 94—109.

Timco, G., Cornett, A., 1999. Is ρ a constant for broken ice rubble?. In: Proceeding of the 10th Workshop on River Ice Management with a Changing Climate, pp. 318—331. Winnipeg, Manitoba, Canada.

Timco, G., Croasdale, K., Wright, B., 2000. An Overview of First-year Sea Ice Ridges. NRC Publications Archive, Canada.

Timco, G., Funke, E., Sayed, M., Laurich, P., 1992. A laboratory apparatus to measure the behaviour of ice rubble. In: Proceedings of Offshore Mechanics and Arctic Engineering Conference, pp. 369—375. Calgary, Canada.

Urroz, G.E., Ettema, R., 1987. Simple-shear box experiments with floating ice rubble. Cold Reg. Sci. Technol. 14, 185—199.

Weiss, R., Prodanovic, A., Wood, K., 1981. Determination of ice rubble shear properties. In: Proceeding of the International Symposium on Ice, pp. 860—872. Quebec, Canada.

Wong, T., Morgenstern, N., Sego, D., 1990. A constitutive model for broken ice. Cold Reg. Sci. Technol. 17, 241—252.